

# One-dimensional projection of two-dimensional systems using spiral boundary conditions

Masahiro Kadosawa,<sup>1</sup> Masaaki Nakamura,<sup>2</sup> Yukinori Ohta,<sup>1</sup> and Satoshi Nishimoto<sup>3,4</sup>

<sup>1</sup>*Department of Physics, Chiba University, Chiba 263-8522, Japan*

<sup>2</sup>*Department of Physics, Ehime University, Ehime 790-8577, Japan*

<sup>3</sup>*Department of Physics, Technical University Dresden, 01069 Dresden, Germany*

<sup>4</sup>*Institute for Theoretical Solid State Physics, IFW Dresden, 01069 Dresden, Germany*

(Dated: February 13, 2023)

We introduce spiral boundary conditions (SBCs) as a useful tool for handling the shape of finite-size periodic clusters. Using SBCs, a lattice model for more than two dimensions can be exactly projected onto a one-dimensional (1D) periodic chain with translational invariance. Hence, the existing 1D techniques such as density-matrix renormalization group (DMRG), bosonization, Jordan–Wigner transformation, etc., can be effectively applied to the projected 1D model. First, we describe the 1D projection scheme for the two-dimensional (2D) square- and honeycomb-lattice tight-binding models in real and momentum space. Next, we discuss how the density of states and the ground-state energy approach their thermodynamic limits. Finally, to demonstrate the utility of SBCs in DMRG simulations, we estimate the magnitude of staggered magnetization of the 2D XXZ Heisenberg model as a function of XXZ anisotropy.

*Introduction.* In condensed matter physics, theoretical research is usually carried out based on the statistical mechanical formulation of either lattice or continuum models which describe the microscopic structure of solids. In general, a lattice model is a cluster of lattice points corresponding to the positions of aligned atoms in a crystal [1]. The Hamiltonian is typically expressed as a countable set of lattice points or bonds, because finite degrees of freedom such as spin, charge, hole, etc are assigned in each lattice point. Therefore, unlike in the continuum limit with huge degrees of freedom, a lattice model is rather suitable for computer simulations. Typical examples of lattice model are the Hubbard model [2], the Heisenberg model [3], the Kondo-lattice model [4], and the Kitaev model [5]. A microscopic starting point to understand the electronic and/or magnetic properties of solids is provided by solving those kinds of lattice models analytically or numerically.

When studying such a model in numerical simulations, we usually put it on a lattice of finite size. Then, an extrapolation of the result to an infinite system is considered if necessary. However, since the total degrees of freedom of the system increases exponentially with lattice size, the geometry of the cluster can be strongly restricted especially for systems in more than two dimensions. In such cases, the management of boundary conditions is crucial to ensure “correct” simulations. Either periodic boundary conditions (PBCs), open boundary conditions (OBCs), or a combination of them, such as e.g., a cylinder, are typically used. Nevertheless, a naive choice of boundary conditions could easily give rise to a situation where the lowest-energy state with a small cluster is not relevant to the ground state (GS) in the thermodynamic limit, instead of systematic errors due to the finite-size effects. This issue could be addressed for example by the sorting of states with, e.g., quantum numbers, momentum, and parity, as explicitly done in level spectroscopy [6], or by controlling the open edges for a particular state [7]. However, these approaches are not always successful.

A simple alternative way to resolve or reduce the above is-

sue is by the use of spiral boundary conditions (SBCs). As explained below, SBCs enable us to represent two-dimensional (2D) lattice sites by a one-dimensional (1D) array. This method was originally used to optimize the computational cost in Monte Carlo simulations [8] but it also allows us to efficiently apply existing 1D techniques such as the density-matrix renormalization group (DMRG) [9], bosonization [10], and Jordan–Wigner transformation [11], etc. SBCs have been also introduced for extending the Lieb–Schultz–Mattis theorem to higher dimensions [12] and for discussing the GS degeneracy in the thermodynamic limit [13]. In this Letter, we thus propose SBCs as a useful tool for handling the shape of finite-size periodic clusters. As practical examples, we describe the 1D projections of the 2D square- and honeycomb-lattice tight-binding (TB) models in real and momentum space. Then, we present how the density of states (DOS) and the GS energy approach their thermodynamic limits. Furthermore, in order to demonstrate the utility of SBCs, we calculate the GS energy of the 2D half-filled Hubbard model and the magnitude of staggered magnetization of the 2D XXZ Heisenberg model using the DMRG method. Their estimations had been longstanding problems and were only recently settled [14, 15]. In our DMRG calculations, we keep up to 12 000 density-matrix eigenstates and the typical discarded weight is smaller than  $\sim 10^{-5}$ . More detailed data are given in the Supplemental Material.

*Projection of 2D cluster onto 1D chain using SBCs.* SBCs are a variation of the idea of PBCs. They provide a way to map lattice models for more than two dimensions onto 1D periodic chains with translation symmetry. As an illustration, let us consider the TB model on a square lattice with  $L_x \times L_y$  sites. When a PBC is applied to its finite-size system, we usually use a rectangular cluster and sites on one edge of the cluster are assumed to be neighbors of the corresponding sites on the opposite edge. However, this choice may be arbitrarily deformed as long as the boundaries have the correct topology of state. Thus, we now make a particular choice of boundaries shown in Fig. 1(a), where all sites are traced along the dashed line

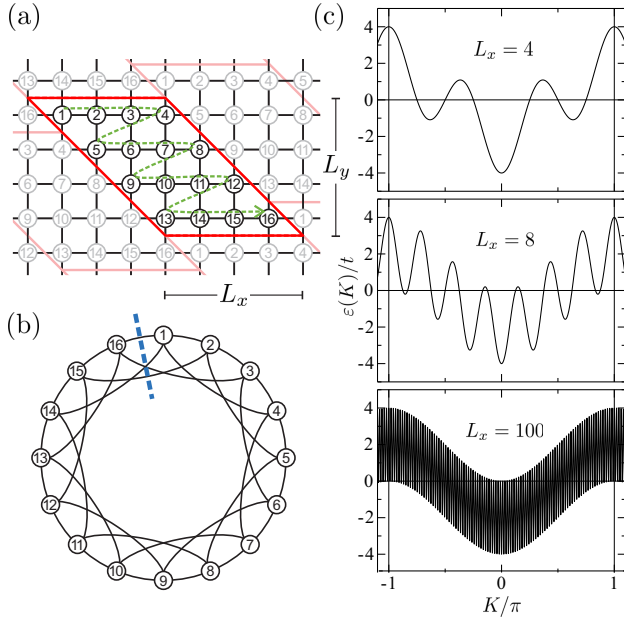


FIG. 1. (a) 2D square-lattice cluster with  $4 \times 4$  sites, where the region framed by the red line is the original cluster. (b) 1D representation of the cluster (a) by numbering sites along the green line. This is a periodic chain, and an open chain is created by cutting  $L_x$  bonds between two sites (dotted line). (c)  $L_x$  dependence of the energy dispersion  $\varepsilon(K)$ , where the limit  $L_y \rightarrow \infty$  is taken.

in a spiral manner. In this way, the original 2D cluster can be exactly reproduced as a 1D chain with nearest- and  $(L_x - 1)$ -th-neighbor hopping integrals [Fig. 1(b)], where the translational symmetry is preserved. The Hamiltonian is written as  $\mathcal{H}_{\text{sq},0} = -t \sum_{\sigma} \sum_{i=1}^{L_x L_y} (c_{i,\sigma}^{\dagger} c_{i+1,\sigma} + c_{i,\sigma}^{\dagger} c_{i+(L_x-1),\sigma} + \text{H.c.})$ , where  $c_{i,\sigma}$  is an annihilation operator of an electron with spin  $\sigma$  at site  $i$ , and  $t$  is the nearest-neighbor hopping integral in the original 2D model. Its Fourier transform leads to  $\mathcal{H}_{\text{sq},K} = -2t \sum_{K,\sigma} [\cos K + \cos(L_x - 1)K] c_{K,\sigma}^{\dagger} c_{K,\sigma}$ , where  $K$  is the momentum defined along the projected 1D periodic chain and  $c_{K,\sigma} = (1/\sqrt{L_x L_y}) \sum_i \exp(iKr_i) c_{i,\sigma}$ . Since the sites are ordered along a "snakelike" path shown in Fig. 1(a), the original 2D momenta  $(k_x, k_y) = \left(\frac{2\pi}{L_x} n_x, \frac{2\pi}{L_y} n_y\right)$  ( $n_x = 0, 1, \dots, L_x - 1; n_y = 0, 1, \dots, L_y - 1$ ) are transferred to the 1D momentum  $K = \frac{2\pi}{L_x L_y} n$  with  $n = n_x + L_x n_y = 0, 1, \dots, L_x L_y - 1$ .

The  $L_x$  dependence of the energy dispersion  $\varepsilon(K) = -2t[\cos K + \cos(L_x - 1)K]$  is shown in Fig. 1(c), where the limit  $L_y \rightarrow \infty$  is taken to obtain a continuous dispersion with  $K$ . Reflecting the snakelike order of sites in the original 2D cluster, the dispersion is oscillating as a function of  $K$ . In the large  $L_x$  limit it turns out to be a beltlike dispersion relation which is interpreted as the projected band structure of the square-lattice TB model onto a Cartesian axis, i.e.,  $x$  or  $y$ . The original 2D Fermi surface is represented as a "Fermi line." For example, when the Fermi level is set at  $0 < \varepsilon_F < 4$ , two separate unoccupied regions correspond to the hole pockets.

Let us see the case of half filling. The dispersion is particle-

hole symmetric and there are  $2L_x - 2$  Fermi points. The GS energy  $E_0$  can be calculated by carrying out the single-particle energy summation over the  $L_x - 1$  regions with  $\varepsilon(K) < 0$ ,

$$\begin{aligned} \frac{E_0}{L_x L_y} &= -\frac{4}{\pi} \int_{\varepsilon(K) < 0} (\cos K + \cos[(L_x - 1)K]) dK \quad (1) \\ &= -\frac{4}{\pi} \sum_{j=1}^{L_x/2} \left[ \sin K + \frac{\sin[(L_x - 1)K]}{L_x - 1} \right]_a^b \quad (2) \\ &\xrightarrow{L_x, L_y \rightarrow \infty} -\frac{16}{\pi^2}, \end{aligned}$$

where  $a = \min(0, \frac{2j-3}{L_x-2}\pi)$  and  $b = \frac{2j-1}{L_x}\pi$ . This energy coincides with that of the infinite-size system. Therefore, we can confirm that the finite-size systems under SBCs are adiabatically connected to the thermodynamic limit. More details are given in the Supplemental Material.

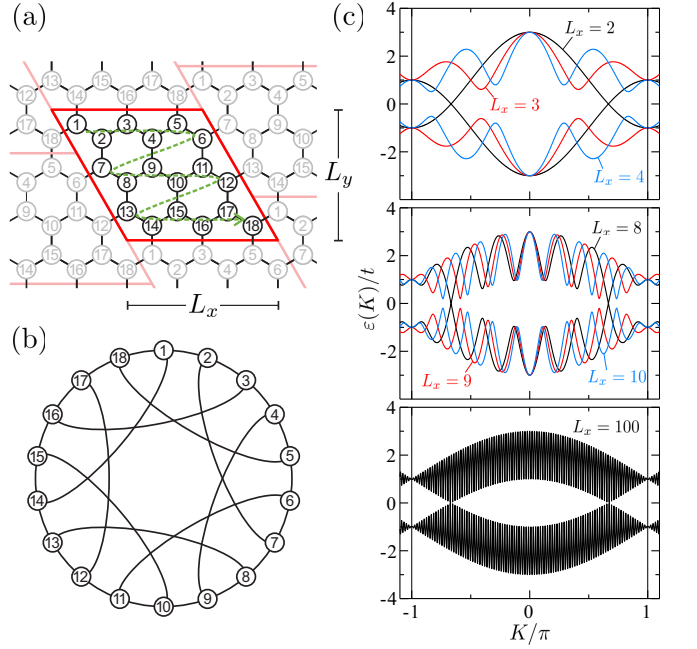


FIG. 2. (a) 2D honeycomb-lattice cluster with  $3 \times 3$  unit cells, where a region framed by the red line is the original cluster. (b) 1D representation of the cluster (a) by numbering sites along the green line. (c)  $L_x$ -dependence of the energy dispersion  $\varepsilon(K)$ , where the limit  $L_y \rightarrow \infty$  is taken. The upper and lower bands are degenerate at  $K = \pm \frac{2}{3}\pi$  when  $2L_x - 1 = 3M$  ( $M$ : integer).

Note that the way of 1D projection using SBCs is not unique. This means that the modulation of the wave function can be controlled more flexibly than PBCs [16]. In other words, a periodic system consistent with an arbitrary commensurate ordering vector can be created by tuning the shape of the finite-size cluster and its alignment. Similar boundary conditions have been used in some numerical calculations to manage a limited periodicity of small clusters [17, 18]. Other examples of SBC usage are given in the Supplemental Material.

*Honeycomb-lattice TB model under SBCs.* Another interesting example is the honeycomb-lattice TB model. The choice of spiral boundaries and the corresponding projected 1D chain are shown in Figs. 2(a) and 2(b), respectively. The Hamiltonian of the projected 1D chain is written as  $\mathcal{H}_{\text{hon},0} = -t \sum_{i=1}^{L_x L_y} \sum_{\sigma} (c_{2i-1,\sigma}^{\dagger} c_{2i,\sigma} + c_{2i,\sigma}^{\dagger} c_{2i+1,\sigma} + c_{2i,\sigma}^{\dagger} c_{2i+(2L_x-1),\sigma} + \text{H.c.})$ . For the limit of  $L_y \rightarrow \infty$  the energy dispersion is written as  $\varepsilon(K) = \pm t \sqrt{1 + 4 \cos^2 \frac{K}{2} + 4 \cos \frac{K}{2} \cos \frac{(2L_x-1)K}{2}}$ . The  $L_x$  dependence of  $\varepsilon(K)$  is shown in Fig. 2(c). The upper and lower bands are degenerate at  $K = \pm \frac{2}{3}\pi$  only when  $2L_x - 1 = 3M$ , where  $M$  is an integer. In the limit of  $L_x, L_y \rightarrow \infty$ , the band structure is equivalent to the projected one of 2D graphene onto a zigzag axis. Accordingly, the Dirac points of the original 2D graphene are reproduced at  $K = \pm \frac{2}{3}\pi$ .

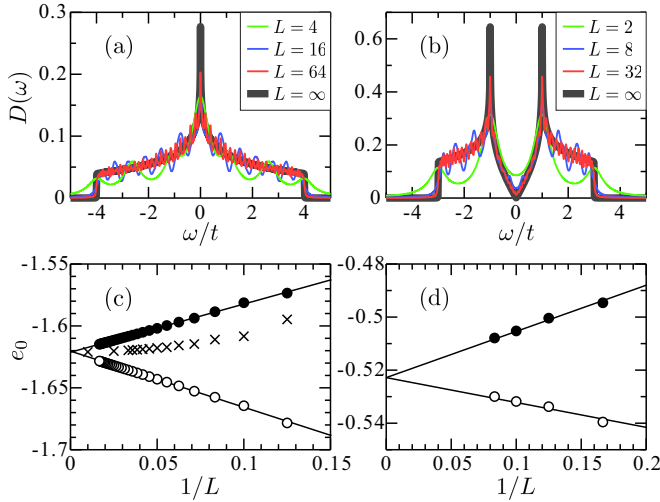


FIG. 3.  $L$  dependence of the density of states for (a) square- and (b) honeycomb-lattice TB models, where a broadening of the  $\delta$  peak  $1.6/L$  and  $0.8/L$  is introduced, respectively. Finite-size scaling analysis of the ground-state energy for the half-filled square-lattice Hubbard model at (c)  $U = 0$  and (d)  $U/t = 8$ . Solid and open circles denote the energy per two bonds and per site calculated with open chains, respectively. Crosses denote the energy per site calculated with periodic chains.

*Approach to the thermodynamic limit.* It is informative to see how the DOS and the GS energy approach their thermodynamic limits. For simplicity, hereafter we consider the case of  $L_x = L_y = L$ . The evolution of the DOS with  $L$  for the square- and honeycomb-lattice TB models is shown in Figs. 3(a) and 3(b), respectively. With increasing  $L$ , they are smoothly connected to the thermodynamic limit ones. Also, the overall shape including the van Hove singularity can be approximately reproduced even with a relatively small cluster. It is because the degeneracy of the energy levels in a finite-size PBC cluster is lifted due to the partial breaking of its rotation symmetry by SBCs. For a square-lattice cluster with  $L \times L$  sites, the number of independent momenta is  $\frac{L^2}{2} + 1$  under SBCs and  $\frac{L^2}{8} + \frac{3L}{4} + 1$  under PBCs. More details are dis-

cussed in the Supplemental Material.

In Fig. 3(c) a finite-size scaling analysis of the GS energy for the half-filled square-lattice TB model with the projected 1D periodic chains is shown. The data points are analytically obtained. As expected, the energy per site ( $e_0$ ) quadratically approaches  $-\frac{16}{\pi^2}$  as a function of  $\frac{1}{L}$ . It is also interesting to see the scaling behavior when open chains are used. An open chain is created by cutting  $L$  bonds between two neighboring sites of the periodic chain [see Fig. 1(b)]. Note though that the number of missing bonds is reduced from  $2L$  in the original 2D PBC cluster to  $L$ . Nevertheless, since the ratio of the number of bonds per site deviates from 2 due to the missing bonds for finite-size open chains, it is convenient to estimate the GS energy in two different ways: One is the energy per site and the other is that per two bonds. As shown in Fig. 3(c), both of them are extrapolated almost linearly to the thermodynamic limit. One of them is extrapolated from the higher-energy side with decreasing  $\frac{1}{L}$  and the other from the lower-energy side, so that this makes the scaling analysis more reliable. Eventually, the scaling behavior with open chains seems to be even more simple than that with periodic chains.

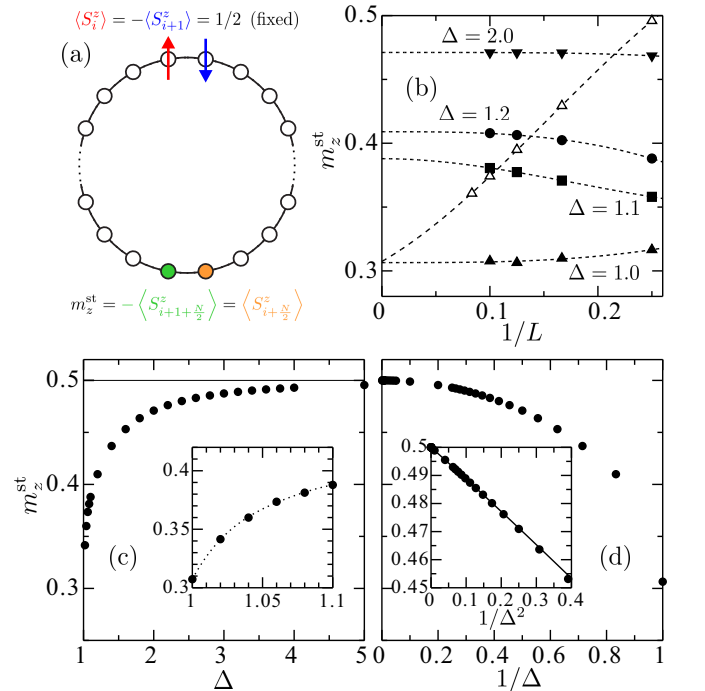


FIG. 4. (a) Schematic picture of the 1D periodic chain used for the DMRG calculations of staggered magnetization  $m_z^{\text{st}}$ . (b) Finite-size scaling analysis of  $m_z^{\text{st}}$ . Solid symbols denote the data points estimated with spin rotation symmetry breaking, and open triangles denote those estimated from the static structure factor (see text). (c), (d) Extrapolated values of  $m_z^{\text{st}}$  in the thermodynamic limit. Insets: Enlarged views near  $\Delta = 1$  and  $1/\Delta = 0$ , respectively. The solid line in the inset of (d) shows a fitting by a polynomial function  $1/\Delta$ .

*Application of SBCs in DMRG calculations.* In DMRG simulations for a 2D system, it is not easy to obtain physi-

cal quantities in the thermodynamic limit because not only are their implementations challenging even with finite-size clusters, but also the finite-size scaling analysis must be performed along two orientations, e.g., the  $x$  and  $y$  directions. This issue can be somewhat alleviated by applying the above 1D projection scheme. In order to demonstrate this, we here present two examples of DMRG simulations for a 2D system.

The first example is the GS energy of the 2D half-filled Hubbard model on a square lattice, whose Hamiltonian is  $\mathcal{H} = \mathcal{H}_{\text{sq},0} + U \sum_i n_{i,\uparrow} n_{i,\downarrow}$ , where  $n_{i,\sigma} = c_{i,\sigma}^\dagger c_{i,\sigma}$ . In Fig. 3(d) the finite-size scaling of GS energy for  $U = 8$  is performed. As is the case in the TB model, open chains are used, so that the extrapolation to the thermodynamic limit seems to be straightforward. It leads to  $e_0 = -0.5228$  by linear fitting. This energy is only slightly higher than  $e_0 = -0.5241$  estimated by DMRG calculations with infinite-length cylinders [14]. Perhaps the extrapolation in the circumferential direction may contain some uncertainty due to the unsettled scaling function with several data points.

The second example is the spontaneous staggered magnetization of the 2D XXZ Heisenberg model on a square lattice, whose Hamiltonian is  $\mathcal{H} = \sum_{\langle i,j \rangle} (S_i^x S_j^x + S_i^y S_j^y + \Delta S_i^z S_j^z)$ , where  $S_i^\gamma$  are the spin- $\frac{1}{2}$  operators associated with site  $i$ ,  $\Delta$  is the anisotropy parameter, and the sum  $\langle i,j \rangle$  runs over all nearest-neighbor pairs. We here use periodic chains. As sketched in Fig. 4(a), the  $z$  components of spins at sites  $i$  and  $i + 1$  are fixed to  $\frac{1}{2}$  and  $-\frac{1}{2}$ , respectively, and the spin moments at the farthest two sites from the fixed spins are measured:  $m_z^{\text{st}} = -\langle S_{i+1+\frac{N}{2}}^z \rangle = \langle S_{i+\frac{N}{2}}^z \rangle$ . Several examples of the finite-size scaling analysis are shown in Fig. 4(b), where the spin moments are calculated using periodic chains with lengths up to  $N = L^2 = 100$  sites. For the isotropic case ( $\Delta = 1$ ), we obtain  $m_z^{\text{st}} = 0.3071 \pm 0.0005$  in the thermodynamic limit. This value is reasonably close to the previous DMRG ( $m_z^{\text{st}} = 0.3067$ ) [19] and quantum Monte Carlo ( $m_z^{\text{st}} = 0.30743$ ) [15] estimations. The magnetization increases with increasing  $\Delta$ . The extrapolated values of  $m_z^{\text{st}}$  are plotted as a function of  $\Delta$  in Fig. 4(c). The overall behavior is basically consistent with the previous studies [20–23]. However, a singularity near  $\Delta = 1$ ,  $m_z^{\text{st}} = \sum_{n=0}^{\infty} \mu_n (1 - \Delta^{-2})^{n/2}$ , predicted by the spin-wave theory [20, 24, 25] is not confirmed in our results. This is consistent with results from the coupled cluster method [23]. A more detailed analysis is given in Ref. [26]. On the other hand, as shown in Fig. 4(d), our data in the large- $\Delta$  region ( $0 \leq 1/\Delta \leq 0.05$ ) can be fitted by  $2m_z^{\text{st}} = 1 + m_2/\Delta^2 + m_4/\Delta^4 + m_6/\Delta^6$  with  $m_2 = -0.222\,222\,225$ ,  $m_4 = -0.035\,554\,273\,6$ , and  $m_6 = -0.018\,966\,381\,0$ . This agrees well with the series expansions  $2m_z^{\text{st}} = 1 - (2/9)/\Delta^2 - (8/225)/\Delta^4 - 0.018\,942\,58/\Delta^6 + \mathcal{O}(1/\Delta^8)$  ( $2/9 = 0.222\,222\,22\dots$ ,  $8/225 = 0.035\,555\,5\dots$ ) [20].

Finally, we present another option to calculate the staggered magnetization. In the above estimations, the spin rotation symmetry is broken by design. Although it makes the DMRG calculations more stable, an equally precise estima-

tion of  $m_z^{\text{st}}$  is also possible without such explicit symmetry breaking. Using open chains, we can accurately estimate the staggered magnetization from the static structure factor  $(m_z^{\text{st}})^2 = \lim_{L \rightarrow \infty} (1/L^2) \sum_{ij} (-1)^{i-j} \langle \mathbf{S}_i \cdot \mathbf{S}_j \rangle$ , where the sum is taken over the open chain. The finite-size scaling analysis using the chains with lengths up to  $12 \times 12$  is given in Fig. 4(b). We obtain  $m_z^{\text{st}} = 0.30762 \pm 0.0032$  in the thermodynamic limit.

*Summary.* Applying SBCs, lattice models for more than two dimensions can be exactly projected onto 1D periodic chains with translational invariance. In the projected 1D chain, each lattice site is indexed by a single coordinate instead of two coordinates in the original 2D PBC cluster, so that we only have to perform a finite-size scaling analysis along the chain direction to obtain a physical quantity in the thermodynamic limit. As practical examples, we first explained how the 2D square- and honeycomb-lattice TB models are expressed as 1D periodic systems in both real and momentum space. Then, the evolution of the DOS with increasing cluster size as well as a finite-size scaling analysis of the GS energy to the thermodynamic limit was shown. Finally, in order to demonstrate the utility of this 1D projection scheme in DMRG simulations, we calculated the magnitude of staggered magnetization in the 2D XXZ Heisenberg model on a square lattice.

The 1D projection scheme using SBCs can be extended to further research. Since the projected 1D chain has translational symmetry, all of the so-called (local)  $A$  tensors are set to be equivalent in a matrix product state. As a result, quantum entanglement is uniformly distributed over the projected 1D chain. It is also important that the distance of the longest bonds is minimized. These conditions enable us to optimally perform DMRG calculations, and also allow us to use the existing techniques such as infinite DMRG and transfer-matrix renormalization group. Though only two kinds of 2D lattices are considered in this Letter, a similar 1D projection is possible for any periodic lattices in more than two dimensions [8]. Moreover, in most cases SBCs are expected to practically give an easier finite-size scaling analysis than the cylinder and PBCs. To clarify the advantages of SBCs in DMRG simulations, the comparison of performance with other boundary conditions is discussed in the Supplemental Material.

*Acknowledgements.* We thank Ulrike Nitzsche for technical support. This work was supported by Grants-in-Aid for Scientific Research from JSPS (Projects No. JP20H01849, No. JP20K03769, and No. JP21J20604). M.K. acknowledges support from the JSPS Research Fellowship for Young Scientists. M.N. acknowledges the Visiting Researcher's Program of the Institute for Solid State Physics, The University of Tokyo, and the research fellow position of the Institute of Industrial Science, The University of Tokyo. S.N. acknowledges support from SFB 1143 project A05 (project-id 247310070) of the Deutsche Forschungsgemeinschaft.

- 
- [1] N. W. Ashcroft and N. D. Mermin, *Solid state physics* (Saunders College Publishing, Philadelphia, 1976).
- [2] J. Hubbard, Electron correlations in narrow energy bands, Proc. R. Soc. London, Ser. A **276**, 238 (1963).
- [3] W. J. Heisenberg, Zur theorie des ferromagnetismus, Zeitschrift für Physik **49**, 619 (1928).
- [4] J. Kondo, Resistance minimum in dilute magnetic alloys, Prog. Theor. Phys. **32**, 37 (1964).
- [5] A. Kitaev, Anyons in an exactly solved model and beyond, Ann. Phys. **321**, 2 (2006).
- [6] K. Okamoto and K. Nomura, Fluid-dimer critical point in  $S = 1/2$  antiferromagnetic Heisenberg chain with next nearest neighbor interactions, Phys. Lett. A **169**, 433 (1992).
- [7] S. Nishimoto and M. Nakamura, Non-symmetry-breaking ground state of the  $S = 1$  Heisenberg model on the kagome lattice, Phys. Rev. B **92**, 140412 (2015).
- [8] M. E. Newman and G. T. Barkema, *Monte Carlo methods in statistical physics* (Clarendon Press, Oxford, UK, 1999).
- [9] S. R. White, Density matrix formulation for quantum renormalization groups, Phys. Rev. Lett. **69**, 2863 (1992).
- [10] A. O. Gogolin, A. A. Nersisyan, and A. M. Tsvelik, *Bosonization and strongly correlated systems* (Cambridge University Press, U.K., 2004).
- [11] H.-D. Chen and Z. Nussinov, Exact results of the Kitaev model on a hexagonal lattice: spin states, string and brane correlators, and anyonic excitations, J. Phys. A: Math. Theor. **41**, 075001 (2008).
- [12] Y. Yao and M. Oshikawa, Generalized boundary condition applied to Lieb-Schultz-Mattis-Type ingappabilities and many-body chern numbers, Phys. Rev. X **10**, 031008 (2020).
- [13] M. G. Yamada and S. Fujimoto, Thermodynamic signature of SU(4) spin-orbital liquid and symmetry fractionalization from lieb-schultz-mattis theorem, Phys. Rev. B **105**, L201115 (2022).
- [14] J. P. F. LeBlanc, A. E. Antipov, F. Becca, I. W. Bulik, G. K.-L. Chan, C.-M. Chung, Y. Deng, M. Ferrero, T. M. Henderson, C. A. Jiménez-Hoyos, E. Kozik, X.-W. Liu, A. J. Millis, N. V. Prokof'ev, M. Qin, G. E. Scuseria, H. Shi, B. V. Svistunov, L. F. Tocchio, I. S. Tupitsyn, S. R. White, S. Zhang, B.-X. Zheng, Z. Zhu, and E. Gull (Simons Collaboration on the Many-Electron Problem), Solutions of the Two-Dimensional Hubbard Model: Benchmarks and Results from a Wide Range of Numerical Algorithms, Phys. Rev. X **5**, 041041 (2015).
- [15] A. W. Sandvik and H. G. Evertz, Loop updates for variational and projector quantum monte carlo simulations in the valence-bond basis, Phys. Rev. B **82**, 024407 (2010).
- [16] M. Nakamura, S. Masuda, and S. Nishimoto, Characterization of topological insulators based on the electronic polarization with spiral boundary conditions, Phys. Rev. B **104**, L121114 (2021).
- [17] Y. Nishiyama, Deconfinement criticality in the spatially anisotropic triangular antiferromagnet with ring exchange, Phys. Rev. B **79**, 054425 (2009).
- [18] A. Miyata, T. Hikihara, S. Furukawa, R. K. Kremer, S. Zherlitsyn, and J. Wosnitza, Magnetoelastic study on the frustrated quasi-one-dimensional spin- $\frac{1}{2}$  magnet LiCuVO<sub>4</sub>, Phys. Rev. B **103**, 014411 (2021).
- [19] S. R. White and A. L. Chernyshev, Néel Order in Square and Triangular Lattice Heisenberg Models, Phys. Rev. Lett. **99**, 127004 (2007).
- [20] Z. Weihong, J. Oitmaa, and C. J. Hamer, Square-lattice Heisenberg antiferromagnet at  $T = 0$ , Phys. Rev. B **43**, 8321 (1991).
- [21] C. J. Hamer, Z. Weihong, and P. Arndt, Third-order spin-wave theory for the Heisenberg antiferromagnet, Phys. Rev. B **46**, 6276 (1992).
- [22] H.-Q. Lin, J. S. Flynn, and D. D. Betts, Exact diagonalization and quantum Monte Carlo study of the spin- $\frac{1}{2}$  XXZ model on the square lattice, Phys. Rev. B **64**, 214411 (2001).
- [23] R. Bishop, P. Li, R. Zinke, R. Darradi, J. Richter, D. Farnell, and J. Schulenburg, The spin-half XXZ antiferromagnet on the square lattice revisited: A high-order coupled cluster treatment, J. Magn. Magn. Mater. **428**, 178 (2017).
- [24] Z. Weihong, J. Oitmaa, and C. J. Hamer, Second-order spin-wave results for the quantum XXZ and XY models with anisotropy, Phys. Rev. B **44**, 11869 (1991).
- [25] D. A. Huse, Ground-state staggered magnetization of two-dimensional quantum Heisenberg antiferromagnets, Phys. Rev. B **37**, 2380 (1988).
- [26] M. Kadosawa, M. Nakamura, Y. Ohta, and S. Nishimoto, Study of staggered magnetization in the spin- $S$  square-lattice Heisenberg model using spiral boundary conditions, J. Phys. Soc. Jpn. **92**, 023701 (2023).

# Supplementary Material for “One-dimensional projection of two-dimensional systems using spiral boundary conditions”

Masahiro Kadosawa<sup>1</sup>, Masaaki Nakamura<sup>2</sup>, Yukinori Ohta<sup>1</sup>, and Satoshi Nishimoto<sup>3,4</sup>

<sup>1</sup> *Department of Physics, Chiba University, Chiba 263-8522, Japan*

<sup>2</sup> *Department of Physics, Ehime University, Ehime 790-8577, Japan*

<sup>3</sup> *Department of Physics, Technical University Dresden, 01069 Dresden, Germany*

<sup>4</sup> *Institute for Theoretical Solid State Physics, IFW Dresden, 01069 Dresden, Germany*

(Dated: February 13, 2023)

Here we present a detailed analysis of the ground-state energy of the half-filled tight-binding model on a square lattice using spiral boundary conditions. We also discuss the difference in the density of states between using periodic and spiral boundary conditions. In addition, the detailed data of our DMRG calculations with spiral boundary conditions are compared to those with various boundary conditions. Finally, possible advantage of spiral boundary conditions in DMRG simulation is discussed.

## GROUND-STATE ENERGY OF THE TIGHT-BINDING MODEL ON A SQUARE LATTICE

Using periodic boundary conditions (PBC), the Hamiltonian of the tight-binding model on a square lattice is written as

$$\mathcal{H}_{0,\text{sq}} = -t \sum_{i,\sigma} (c_{(x,y),\sigma}^\dagger c_{(x+1,y),\sigma} + c_{(x,y),\sigma}^\dagger c_{(x,y+1),\sigma} + \text{H.c.}) \quad (\text{S1})$$

where  $c_{(x,y),\sigma}$  is an annihilation operator of electron with spin  $\sigma$  at site  $(x, y)$ ,  $t$  is nearest-neighbor hopping integral, and  $c_{(x,y),\sigma} = c_{(x+n_x L_x, y+n_y L_y),\sigma}$ , where  $n_x$  and  $n_y$  are integers. The Fourier transform of (S1) reads

$$\mathcal{H}_{\text{sq},\mathbf{k}} = -2t \sum_{\mathbf{k},\sigma} (\cos k_x + \cos k_y) c_{\mathbf{k},\sigma}^\dagger c_{\mathbf{k},\sigma} \quad (\text{S2})$$

where  $c_{\mathbf{k},\sigma} = \frac{1}{\sqrt{L_x L_y}} \sum_{x,y} \exp(i\mathbf{k} \cdot \mathbf{r}) c_{(x,y),\sigma}$  with  $\mathbf{r} = (x, y)$  and  $\mathbf{k} = (k_x, k_y) = \left(\frac{2\pi}{L_x} m_x, \frac{2\pi}{L_y} m_y\right)$  [ $m_x = 0, 1, \dots, L_x - 1$ ;  $m_y = 0, 1, \dots, L_y - 1$ ]. In the thermodynamic limit the ground-state energy at half filling is given by

$$e_0 = \frac{-2t}{(2\pi)^2} \int \int_{\varepsilon(K) < 0} dk_x dk_y (\cos k_x + \cos k_y) = -\frac{16}{\pi^2} t. \quad (\text{S3})$$

As explained in the main text, using spiral boundary conditions (SBC) the original two-dimensional (2D) square-lattice cluster with  $L_x \times L_y$  sites can be exactly reproduced as a one-dimensional (1D) chain with nearest- and  $(L_x - 1)$ -th neighbor hopping integrals, where the translational symmetry is preserved. The Hamiltonian is written as

$$\mathcal{H}_{0,\text{sq}} = -t \sum_{\sigma} \sum_{i=1}^{L_x L_y} (c_{i,\sigma}^\dagger c_{i+1,\sigma} + c_{i,\sigma}^\dagger c_{i+(L_x-1),\sigma} + \text{H.c.}), \quad (\text{S4})$$

where  $c_{i,\sigma}$  is an annihilation operator of electron with spin  $\sigma$  at site  $i$ . Its Fourier transform leads to

$$\mathcal{H}_{\text{sq},K} = -2t \sum_{K,\sigma} (\cos K + \cos(L_x - 1)K) c_{K,\sigma}^\dagger c_{K,\sigma}, \quad (\text{S5})$$

where  $c_{K,\sigma} = (1/\sqrt{L_x L_y}) \sum_i \exp(iKr_i) c_{i,\sigma}$ , and the momentum  $K$  is defined along the projected 1D periodic chain as  $K = \frac{2\pi}{L_x L_y} n$  with  $n = n_x + L_x n_y = 0, 1, \dots, L_x L_y - 1$ .

The energy dispersion (S5) for  $L_x = 8$  and  $L_y \rightarrow \infty$  is shown in Fig. S1. Let us then calculate the ground-state energy at half filling, where the shaded areas are occupied by electrons. Since  $\cos K + \cos(L_x - 1)K = 2 \cos \frac{L_x K}{2} \cos \frac{(L_x - 2)K}{2}$ ,

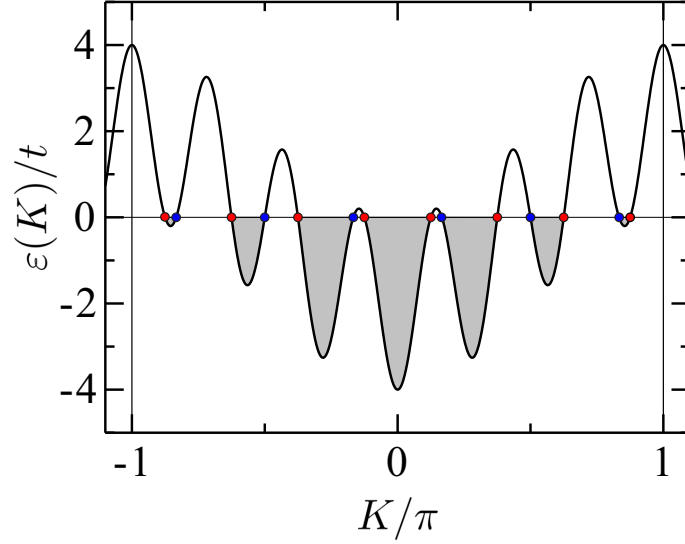


FIG. S1: Energy dispersion of the tight-binding model on a square lattice with spiral boundary conditions, where  $L_x = 8$  and  $L_y \rightarrow \infty$  are taken. At half filling the shaded areas are occupied by electrons.

the Fermi points denoted by red and blue circles are given as

$$\frac{L_x K_r}{2} = \frac{\pi}{2} + n_r \pi \longrightarrow K_r = \frac{\pi}{L_x} (2n_r - 1) \quad (\text{S6})$$

$$\frac{(L_x - 2) K_b}{2} = \frac{\pi}{2} + n_b \pi \longrightarrow K_b = \frac{\pi}{L_x - 2} (2n_b - 1), \quad (\text{S7})$$

respectively, where  $n_r, n_b = 1, 2, \dots$ , Thus,

$$\begin{aligned} e_0 &= \frac{-2t}{\pi} \int_{\varepsilon(K) < 0} dK (\cos K + \cos(L_x - 1)K) \\ &= \frac{-4t}{\pi} \int_0^\pi dK (\cos K + \cos(L_x - 1)K) \theta(-\varepsilon(K)) \\ &= \frac{-4t}{\pi} \left( \left[ \sin K + \frac{\sin[(L_x - 1)K]}{L_x - 1} \right]_0^{\frac{\pi}{L_x}} + \left[ \sin K + \frac{\sin[(L_x - 1)K]}{L_x - 1} \right]_{\frac{\pi}{L_x - 2}}^{\frac{3\pi}{L_x}} + \dots + \left[ \sin K + \frac{\sin[(L_x - 1)K]}{L_x - 1} \right]_{\frac{(L_x - 3)\pi}{L_x - 2}}^{\frac{(L_x - 1)\pi}{L_x}} \right) \\ &= \frac{-4t}{\pi} \left[ \left( \sin \frac{\pi}{L_x} + \sin \frac{3\pi}{L_x} + \dots + \sin \frac{(L_x - 1)\pi}{L_x} \right) + \frac{1}{L_x - 1} \left( \sin \frac{(L_x - 1)\pi}{L_x} + \sin \frac{3(L_x - 1)\pi}{L_x} + \dots + \sin \frac{(L_x - 1)^2 \pi}{L_x} \right) \right. \\ &\quad \left. - \left( \sin \frac{\pi}{L_x - 2} + \sin \frac{3\pi}{L_x - 2} + \dots + \sin \frac{(L_x - 3)\pi}{L_x - 2} \right) \right. \\ &\quad \left. - \frac{1}{L_x - 1} \left( \sin \frac{(L_x - 1)\pi}{L_x - 2} + \sin \frac{3(L_x - 1)\pi}{L_x - 2} + \dots + \sin \frac{(L_x - 3)(L_x - 1)\pi}{L_x - 2} \right) \right]. \quad (\text{S8}) \end{aligned}$$

Applying the formula  $\sin x + \sin(3x) + \dots + \sin[(2n - 1)x] = \frac{1 - \cos(2nx)}{2 \sin x}$  to Eq. (S8), we obtain

$$e_0 = \frac{-4t}{\pi} \left( \frac{1}{\sin \frac{\pi}{L_x}} + \frac{1}{(L_x - 1) \sin \left( \frac{L_x - 1}{L_x} \pi \right)} - \frac{1}{\sin \frac{\pi}{L_x - 2}} - \frac{1}{(L_x - 1) \sin \left( \frac{L_x - 1}{L_x - 2} \pi \right)} \right) \quad (\text{S9})$$

$$\xrightarrow{L_x \gg 1} \frac{-4t}{\pi} \left( \frac{L_x}{\pi} + \frac{L_x}{\pi(L_x - 1)} - \frac{L_x - 2}{\pi} + \frac{L_x - 2}{\pi(L_x - 1)} \right) \xrightarrow{L_x \rightarrow \infty} -\frac{16}{\pi^2}. \quad (\text{S10})$$

This coincides with Eq. (S3). Thus, we can confirm that the finite-size systems under SBC are adiabatically connected to the thermodynamic limit.

SPLITTING OF THE DEGENERATE ENERGY LEVELS BY SPIRAL BOUNDARY CONDITIONS

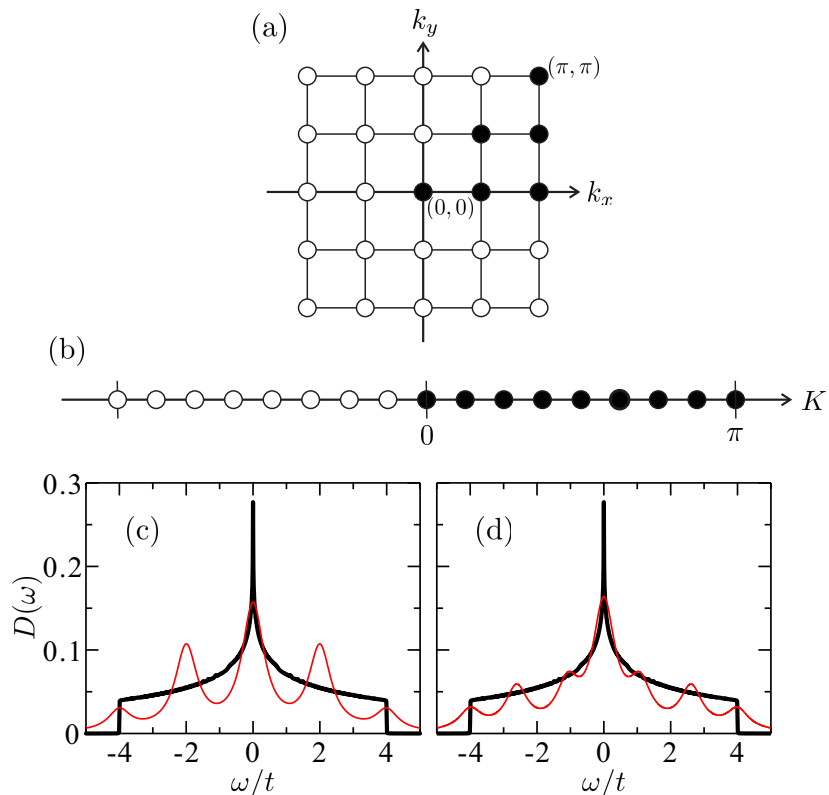


FIG. S2: (a,b) Possible momenta for a  $4 \times 4$  square-lattice cluster under periodic and spiral boundary conditions, respectively. Example sets of independent momenta are denoted by filled circles. (c,d) Density of states for the square-lattice tight-binding model with a  $4 \times 4$  sites with periodic and spiral boundary conditions, respectively.

The symmetries of cluster are different between using SBC and periodic boundary conditions (PBC). Let us here explain it by taking a square-lattice cluster as an example. A cluster with  $L \times L$  sites has a  $C_4$  rotational symmetry under PBC. Accordingly, the number of independent momenta is  $\frac{L^2}{8} + \frac{3L}{4} + 1$ . On the other hand, when SBC are applied, the rotational symmetry is reduced from  $C_4$  to  $C_2$  due to the splitting of the degenerate energy levels. Then, the number of independent momenta is increased to  $\frac{L^2}{2} + 1$ . In Fig. S2(a,b), possible momenta for a  $4 \times 4$  cluster under PBC and SBC are shown, and the independent ones denoted by filled circles are 6 and 9, respectively. As a result, the density of states with SBC is closer to the thermodynamic limit one, see Fig. S2(c,d).

## FLEXIBILITY OF SPIRAL BOUNDARY CONDITIONS

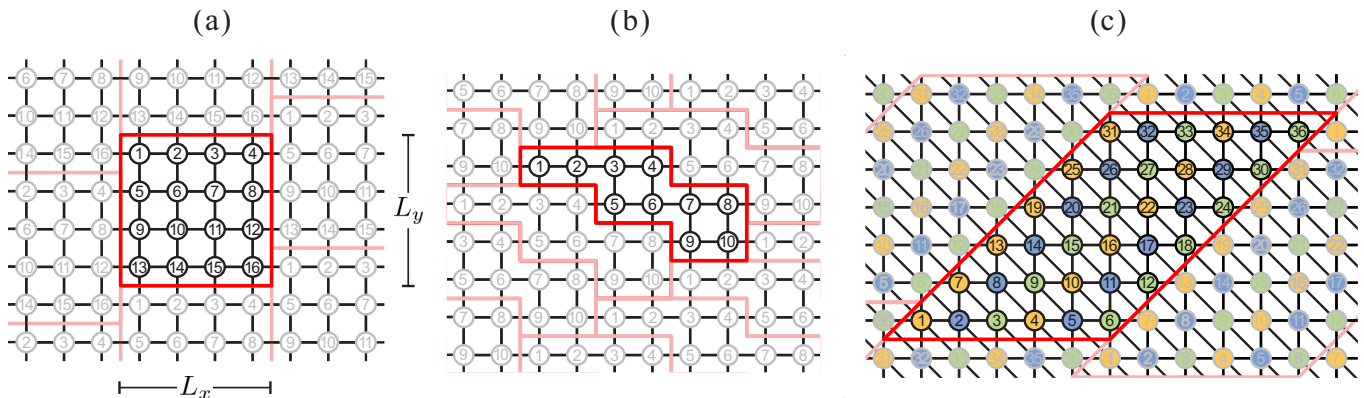


FIG. S3: (a) 2D square-lattice cluster where a region framed by red line is the original cluster. This application of SBC is consistent with an ordered state with modulation of  $\mathbf{k} = (\pi, 0)$ . (b) A possible application of SBC for 10-site non-rectangular cluster. (c) 2D triangular-lattice cluster where a region framed by red line is the original cluster. This application of SBC is consistent with an ordered state with modulation of  $\mathbf{k} = (2\pi/3, 2\pi/3)$ . The sites belonging to different sublattices are color-coded.

As noted in the main text, the way of 1D projection using SBC is not unique [1]. This means that the modulation of wave function can be controlled more flexibly than PBC. The way used for 2D square lattice in the main text is appropriate to study a state with modulation of  $\mathbf{k} = (\pi, \pi)$ , like a Néel state. However, if we study a state with modulation of  $\mathbf{k} = (\pi, 0)$ , it is more convenient to use another application way of SBC. It is shown in Fig. S3(a). In this way, the original 2D square-lattice cluster with  $L_x \times L_y$  sites can be exactly mapped onto a 1D chain with nearest- and  $L_x$ -th neighbor hopping integrals, where the translation symmetry is also preserved. The Hamiltonian is written as

$$\mathcal{H}_{0,\text{sq}} = -t \sum_{\sigma} \sum_{i=1}^{L_x L_y} (c_{i,\sigma}^{\dagger} c_{i+1,\sigma} + c_{i,\sigma}^{\dagger} c_{i+L_x,\sigma} + \text{H.c.}), \quad (\text{S11})$$

and its Fourier transform leads to

$$\mathcal{H}_{\text{sq},K} = -2t \sum_{K,\sigma} (\cos K + \cos L_x K) c_{K,\sigma}^{\dagger} c_{K,\sigma}, \quad (\text{S12})$$

where  $n = n_x + L_x n_y = 0, 1, \dots, L_x L_y - 1$ ). It is interesting that both  $\mathbf{k} = (\pi, \pi)$  in Fig. 1(a) of the main text and  $\mathbf{k} = (\pi, 0)$  in Fig. S3(a) are represented by a  $k = \pi$  modulation in the projected 1D chain.

In fact, when we apply SBC, there is in general no reason to stick to lattices which are square, rectangle, or parallelogram. A cluster shape and number of sites can be relatively-flexibly chosen under SBC. For instance, we can construct a lattice with 10 sites as shown in Fig. S3(b). We can easily confirm that the mapped 1D chain has nearest- and 2nd neighbor bonds and the translational symmetry is preserved. Thus, we are allowed to control the application way of SBC depending on considered physics.

As another example, let us consider a state with modulation of  $\mathbf{k} = (2\pi/3, 2\pi/3)$ . This corresponds to a  $120^\circ$  structure in the triangular-lattice Heisenberg model. Similarly, this state can be represented by 1D chain with translation symmetry, as shown in Fig. S3(c). For a cluster with  $L_x \times L_y$  sites, the 2D system can be exactly mapped onto a 1D chain with nearest-,  $(L_x - 2)$ -th, and  $(L_x - 1)$ -th neighbor bonds.

As shown above, the modulation of cluster can be flexibly controlled. In the case of incommensurate order, it would be able to make a convergence of physical quantity to the thermodynamic limit faster by realizing a possibly closest modulation to the incommensurate vector.

[1] M. Nakamura, S. Masuda, and S. Nishimoto, Characterization of topological insulators based on the electronic polarization with spiral boundary conditions, Phys. Rev. B **104**, L121114 (2021).

## CORRELATION FUNCTIONS FOR VARIOUS BOUNDARY CONDITIONS

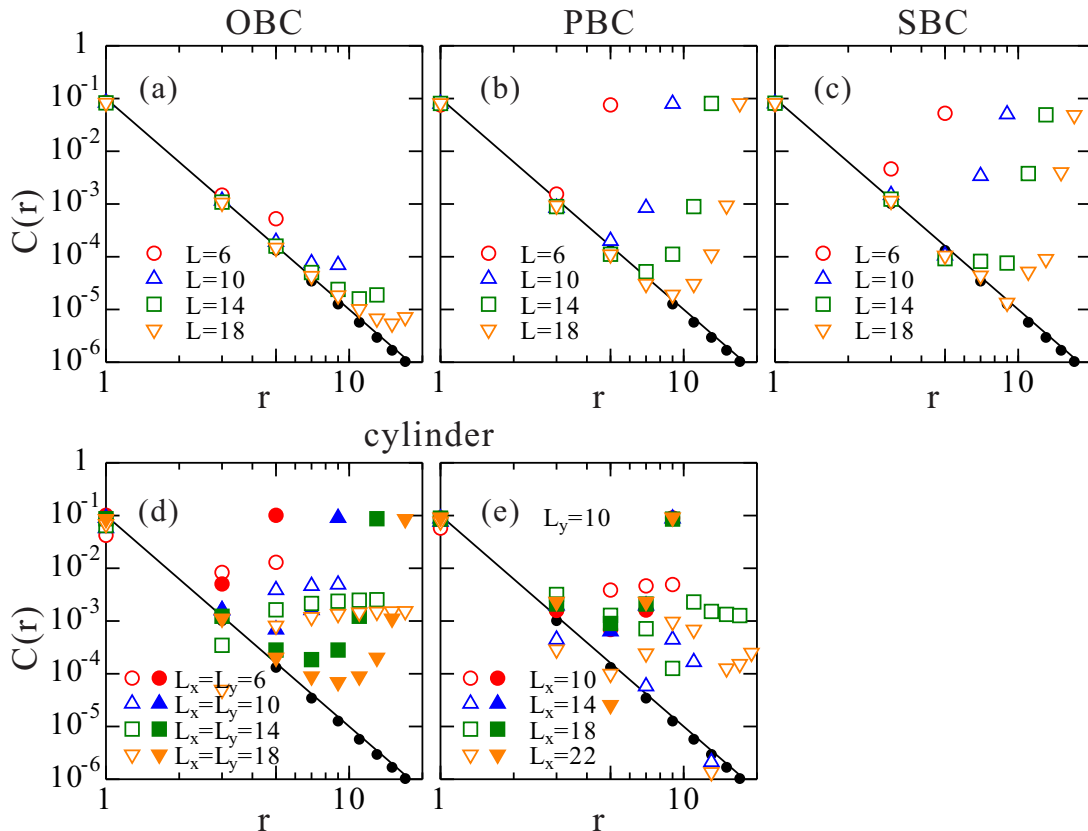


FIG. S4: Density-density correlation functions  $C(r)$  for non-interacting fermions on a 2D square lattice at half filling as a function of distance  $r$  along bond direction, namely,  $(1,0)$  or  $(0,1)$ , with (a) OBC, (b) PBC, (c) SBC, and (d,e) cylinder. For cylinder, the values for both  $(1,0)$  and  $(0,1)$  directions are shown. As a reference data, the result for very large system with  $100 \times 100$  OBC cluster is plotted by black dots. As expected, it decays like  $C(r) \propto 1/r^4$  (black line).

It is interesting to see how correlation functions are affected by boundary conditions. To investigate their long-range behavior, we consider the density-density correlation functions  $C(r) = 1 - \langle n_i n_{i+r} \rangle$  of non-interacting fermions on a 2D square lattice because they can be exactly obtained. In Fig. S4 we plot  $C(r) = 1 - \langle n_i n_{i+r} \rangle$  as a function of distance  $r$  along bond direction, namely,  $(1,0)$  or  $(0,1)$ , at half filling for various boundary conditions. We find that OBC, PBC, and SBC can provide equally good results: For example, the data points up to  $r \sim 9$  are almost on the analytical line  $C(r) \propto 1/r^4$  for the systems with  $L = 18$ . On the other hand, the result with cylindrical cluster is obviously worst, namely, the deviation from  $C(r) \propto 1/r^4$  is largest. As is well known [1], the result seems to be improved by increasing the system size with keeping the ratio between system length and circumference. Nevertheless, the behavior  $C(r) \propto 1/r^4$  can be confirmed only up to  $r \sim 5$  in the case of  $L_x = L_y = 18$  [see Fig. S4(d)]. It is because that cylindrical boundary conditions impose a kind of spatial anisotropy on the original isotropic 2D square-lattice cluster. Furthermore, surprisingly, the result cannot be improved by increasing the system length if the circumference is kept [Fig. S4(e)].

As discussed above, we may choose either OBC or SBC when correlation functions for 2D system are studied. However, a 2D system under OBC can be easily disturbed by Friedel oscillations once it is doped or any interaction is switched on. Therefore, SBC could be a first choice for DMRG study of correlation functions for 2D systems.

[1] A.W. Sandvik, Finite-size scaling and boundary effects in two-dimensional valence-bond solids, Phys. Rev. B **85**, 134407 (2012).

## SIZE SCALING OF GROUND-STATE ENERGY FOR VARIOUS BOUNDARY CONDITIONS

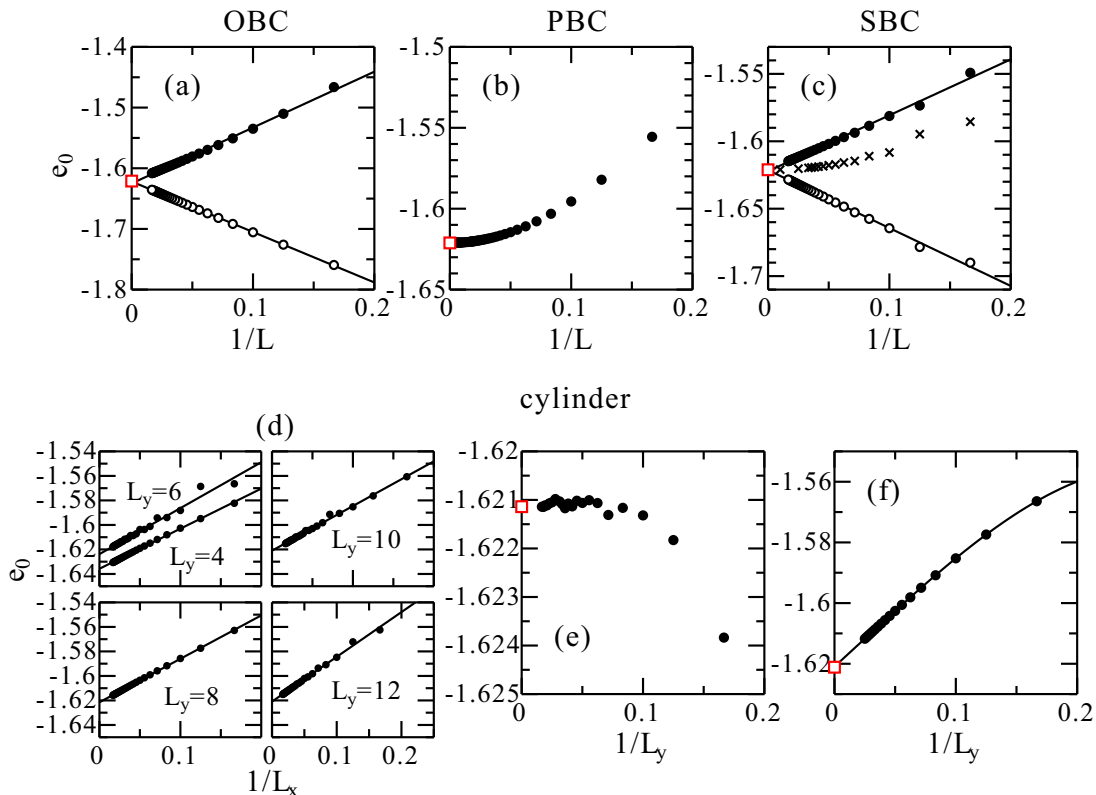


FIG. S5: Finite-size-scaling analysis of the ground-state energy for non-interacting fermions on a 2D square lattice at half filling with (a) OBC, (b) PBC, (c) SBC, and (d-f) cylinder. The exact ground-state energy in the thermodynamic limit,  $e_0 = -16/\pi^2$ , is denoted by red square. The solid and open circles denote the ground state energy per site and per two bonds, respectively. For cylinder, scaling analyses along system length  $L_x$  for given circumferences  $L_y$  are performed in (d), and then scaling analysis along circumference direction is performed in (e), where the extrapolated values obtained in (d) are used. Also, scaling analysis with keeping  $L_x = L_y$  is performed in (f).

We here look into finite-size-scaling behavior of the ground-state energy for each of boundary conditions. In Fig. S5 we perform finite-size-scaling analyses of the ground-state energy for non-interacting fermions on a 2D square lattice at half filling with various boundary conditions. Note that the result for SBC [Fig. S5(c)] is equivalent to Fig. 3(c) in the main text. The scaling behavior for OBC is straightforward [Fig. S5(a)], which is similar to that for the case of 1D projected open chain under SBC [Fig. S5(c)]. On the other hand, the ground-state energy approaches to its thermodynamic-limit value as  $1/L^2$  for PBC. If we use DMRG, the ground-state energies can be calculated only for  $L \lesssim 10$  with 2D periodic clusters. Thus, the finite-size-scaling analysis of the ground-state energy would be difficult for PBC.

When we use cylinder, finite-size-scaling analysis must be performed along two orientations, e.g.,  $x$ - and  $y$ -directions. First, the scaling analyses along system length  $L_x$  for given circumferences  $L_y$  are performed to obtain the  $L_x \rightarrow \infty$  values of the ground-state energy for each  $L_y$  [Fig. S5(d)]. Next, with using the obtained  $L_x \rightarrow \infty$  values further scaling analysis along circumference direction  $L_y$  is performed [Fig. S5(e)]. Similarly to the case of PBC, the scaling behavior looks like  $e_0 = -16/\pi^2 + \alpha/L_y^\beta$  ( $\alpha < 0$ ,  $\beta > 2$ ). Therefore, accurate estimation of the ground-state energy for 2D itinerant systems using DMRG with cylindrical clusters may be not very practical, considering that there would be some uncertainty in the extrapolation to  $L_x \rightarrow \infty$  and the extrapolated values can be obtained only for  $L_y \lesssim 10$ . We also perform a scaling analysis with keeping  $L_x = L_y$  in Fig. S5(f). The scaling behavior looks simple but deviates from a linear function like for OBC and open chain under SBC.

For the above reason, OBC or SBC would be a best choice for estimating the ground-state energy of 2D systems in the thermodynamic limit.

**CONVERGENCE CHECK OF DMRG CALCULATIONS**

TABLE I: Discarded weight  $w_d$  and the ground-state energy  $E_0(m)$  of the half-filled square-lattice Hubbard model at  $U/t = 8$  as functions of system size  $L \times L$  and the number of density-matrix eigenstates kept in the renormalization  $m$ , where SBC are applied. The ground-state energy at  $m \rightarrow \infty$  was obtained by a linear fit of  $E_0(m)$  vs.  $w_d$ .

$L = 6$				$L = 8$			
$m$	$w_d$	$E_0(m)$	$E_0(m) - E_0(\infty)$	$m$	$w_d$	$E_0(m)$	$E_0(m) - E_0(\infty)$
2000	3.432e-06	-17.79364790	0.01227902	2000	1.286e-05	-31.76311291	0.26322934
4000	7.856e-07	-17.80326286	0.00266406	4000	8.420e-06	-31.87302879	0.15331346
6000	3.052e-07	-17.80489349	0.00103344	6000	5.681e-06	-31.91448613	0.11185612
8000	1.516e-07	-17.80541043	0.00051649	8000	4.550e-06	-31.93686464	0.08947761
10000	8.614e-08	-17.80563244	0.00029448	10000	4.165e-06	-31.95093410	0.07540815
12000	5.332e-08	-17.80574150	0.00018542	12000	3.815e-06	-31.96253340	0.06380885
$\infty$		-17.80592692		$\infty$		-32.02634225	

$L = 10$				$L = 12$			
$m$	$w_d$	$E_0(m)$	$E_0(m) - E_0(\infty)$	$m$	$w_d$	$E_0(m)$	$E_0(m) - E_0(\infty)$
2000	2.119e-05	-49.50077175	1.02132882	2000	-	-	-
4000	1.379e-05	-49.84727132	0.67482925	4000	1.840e-05	-71.40452905	1.73164686
6000	1.198e-05	-49.99628942	0.52581115	6000	1.486e-05	-71.71734724	1.41882867
8000	9.848e-06	-50.09485526	0.42724531	8000	1.365e-05	-71.91712273	1.21905318
10000	7.774e-06	-50.15642914	0.36567143	10000	1.224e-05	-72.06942431	1.06675160
12000	5.854e-06	-50.19615496	0.32594561	12000	9.293e-06	-72.19219444	0.94398147
$\infty$		-50.52210057		$\infty$		-73.13617591	

We here check the accuracy of DMRG calculations under SBC (periodic chain). In Table I the discarded weight  $w_d$  and the ground-state energy  $E_0(m)$  of the half-filled square-lattice Hubbard model at  $U/t = 8$  are shown as a function of the number of density-matrix eigenstates kept in the renormalization  $m$  for various system sizes  $L \times L$ . For all cases the ground-state energy at  $m \rightarrow \infty$  ( $w_d \rightarrow 0$ ) can be accurately obtained by a linear fit of  $E_0(m)$  vs.  $w_d$ . We also find that the discarded weight is roughly proportional to  $L$ , i.e.,  $w_d \propto L$ . Nevertheless, the discarded weight is still order of  $\sim 10^{-5}$  even for  $12 \times 12$ . This may fall into the category of an accurate DMRG calculation for 2D fermionic system.

In Table II the discarded weight in the DMRG calculation for the square-lattice Heisenberg model is compared between various boundary conditions. The discarded weight is almost comparable for OBC and cylinder, and somewhat larger for the SBC-projected periodic chain. Surprisingly, it is much smaller when the SBC-projected open chain is studied. Thus, from the viewpoint of discarded weight, OBC, SBC, and cylinder can be equally good options in DMRG calculation for 2D systems

TABLE II: Discarded weight  $w_d$  and the ground-state energy  $E_0(m)$  of the square-lattice Heisenberg model as a function of the number of density-matrix eigenstates kept in the renormalization  $m$  for system sizes  $6 \times 6$  ( $L = 6$ ) and  $8 \times 8$  ( $L = 8$ ) with various boundary conditions. The ground-state energy at  $m \rightarrow \infty$  was obtained by a linear fit of  $E_0(m)$  vs.  $w_d$ .

OBC						
$m$	$L = 6$			$L = 8$		
	$w_d$	$E_0(m)$	$E_0(m) - E_0(\infty)$	$w_d$	$E_0(m)$	$E_0(m) - E_0(\infty)$
1000	1.100e-07	-21.72673267	0.00005340	8.166e-06	-39.60759545	0.01078493
2000	6.466e-09	-21.72678301	0.00000307	1.587e-06	-39.61627493	0.00210544
3000	9.883e-10	-21.72678556	0.00000051	5.714e-07	-39.61762743	0.00075294
4000	2.279e-10	-21.72678592	0.00000015	2.636e-07	-39.61803809	0.00034228
		-21.72678607			-39.61838038	

PBC						
$m$	$L = 6$			$L = 8$		
	$w_d$	$E_0(m)$	$E_0(m) - E_0(\infty)$	$w_d$	$E_0(m)$	$E_0(m) - E_0(\infty)$
1000	2.981e-05	-24.40302953	0.03665799	-	-	-
2000	9.188e-06	-24.42949472	0.01019281	-	-	-
3000	3.938e-06	-24.43541285	0.00427468	-	-	-
4000	1.982e-06	-24.43743236	0.00225516	-	-	-
		-24.43968752				

SBC (periodic chain)						
$m$	$L = 6$			$L = 8$		
	$w_d$	$E_0(m)$	$E_0(m) - E_0(\infty)$	$w_d$	$E_0(m)$	$E_0(m) - E_0(\infty)$
1000	9.130e-06	-24.45300594	0.00801971	9.025e-05	-42.79118365	0.32899812
2000	1.661e-06	-24.45965335	0.00137230	4.565e-05	-42.96307806	0.15710371
3000	5.365e-07	-24.46058729	0.00043835	2.898e-05	-43.02157949	0.09860228
4000	2.260e-07	-24.46083548	0.00019017	1.973e-05	-43.05183014	0.06835163
$\infty$		-24.46102565			-43.12018177	

SBC (open chain)						
$m$	$L = 6$			$L = 8$		
	$w_d$	$E_0(m)$	$E_0(m) - E_0(\infty)$	$w_d$	$E_0(m)$	$E_0(m) - E_0(\infty)$
1000	1.037e-09	-23.07464567	0.00000050	9.819e-07	-41.31375095	0.00116164
2000	2.447e-11	-23.07464616	0.00000001	1.161e-07	-41.31476448	0.00014811
3000	2.351e-12	-23.07464617	$< 10^{-8}$	2.987e-08	-41.31487486	0.00003773
4000	3.837e-13	-23.07464618	$< 10^{-8}$	1.058e-08	-41.31489881	0.00001379
$\infty$		-23.07464618			-41.31491259	

cylinder						
$m$	$L = 6$			$L = 8$		
	$w_d$	$E_0(m)$	$E_0(m) - E_0(\infty)$	$w_d$	$E_0(m)$	$E_0(m) - E_0(\infty)$
1000	3.349e-08	-23.09009340	0.00001678	4.299e-06	-41.34358356	0.00569929
2000	1.512e-09	-23.09010942	0.00000076	7.206e-07	-41.34831869	0.00096415
3000	2.012e-10	-23.09011008	0.00000010	2.330e-07	-41.34898086	0.00030198
4000	4.556e-11	-23.09011016	0.00000002	9.196e-08	-41.34916154	0.00012131
$\infty$		-23.09011018			-41.34928284	

## ADVANTAGES OF SPIRAL BOUNDARY CONDITIONS

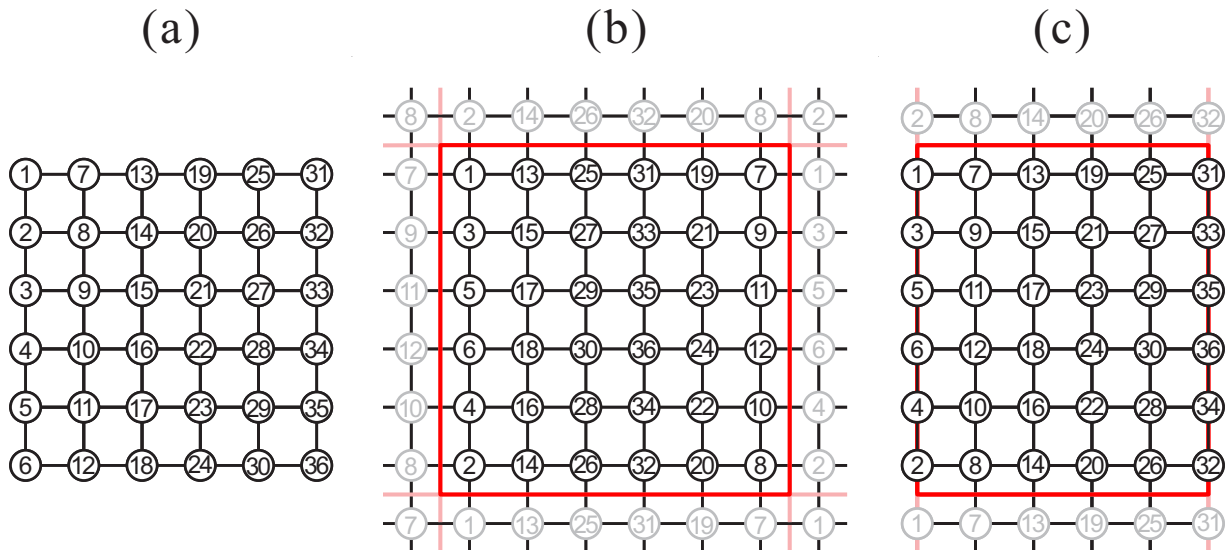


FIG. S6: 2D square-lattice  $6 \times 6$  cluster with (a) OBC, (b) PBC, and (c) cylinder. In each cluster an optimal order of sites for DMRG simulation is denoted by numbers.

In DMRG simulations we have to choose a proper boundary condition for considered system and quantities. The applicability of DMRG to a lattice system can be roughly judged by the distance between two sites connected by the longest-range term in the system. The distance is denoted by  $d$  below. In general, the DMRG calculation is difficult if  $d$  is larger than  $\sim 10$ . Let us then estimate the values of  $d$  for various boundary conditions. In Fig. S6 an optimal order of sites to give the shortest  $d$  for a 2D square-lattice cluster is illustrated for each boundary condition. When we use OBC or cylinder,  $d$  is  $L$  for a  $L \times L$  cluster. This is comparable to that for SBC ( $d = L - 1$  or  $d = L$ ). However, if we use PBC,  $d$  jumps to  $2L$ . This is definitely ill-conditioned for DMRG treatments. For example, the system size is limited up to  $L \sim 6$  in the Heisenberg model. Therefore, PBC may be firstly excluded from the choice, although it is naively thought to be a most versatile boundary condition in numerical calculations.

In fact, either OBC or cylinder is typically employed in the previous DMRG simulations. These boundary conditions are technically rather convenient for DMRG simulations because the value of  $d$  can be reduced down to  $L$  with the optimal order of sites. Nevertheless, they could often lead to some sorts of problems in the physical properties. The followings are examples of issues: With OBC, the bulk state can be significantly disturbed by Friedel oscillations, and also the properties of bulk and edge states can be completely different due to the missing outside bonds especially in doped systems. These problems could be managed by controlling open edges for a specific states, and however, it is not always successful. With cylinder, a kind of spatial anisotropy is introduced in spite of the original isotropic 2D square-lattice cluster. A most problematic point is that short loops of bonds are formed along the circumference direction. This could results in an unnatural periodicity of the wave function as well as an unexpected plaquette constraint of particles or spins. Accordingly, as shown in the previous section of Supplemental Material, the density-density correlation functions can be largely disturbed by cylindrical boundary.

With SBC, Friedel oscillations can be avoidable and no artificial short loops of bonds are created. Also,  $d$  is only  $L$  or  $L - 1$ . Furthermore, a SBC-projected chain with open boundary is used, the accuracy of DMRG calculation is even better than that with OBC and cylinder as shown in the previous section of Supplemental Material. Thus, SBC enables us to perform accurate DMRG calculations with skirting some sorts of finite-size effects seen in OBC and cylindrical clusters. However, we expect that SBC does not always provide better results. For example, OBC may be more appropriate to study a system exhibiting valence-bond-solid state such as plaquette/bond order; and, a cylindrical cluster may be more appropriate to study a system exhibiting magnetic/charge/bond ordered state with spatial rotation symmetry breaking.

We thus think that SBC can be a main option of the boundary conditions in DMRG calculations for the above technical and physical reasons.